J. Fluid Mech. (1984), *vol.* 145, *pp.* 377–403
Printed in Great Britain

Transition to geostrophic turbulence in a rotating differentially heated annulus of fluid

By G. BUZYNA†, R. L. PFEFFER‡ AND R. KUNG†
Florida State University, Tallahassee, FL 32306

(Received 24 May 1983 and in revised form 27 March 1984)

Results are presented of an experimental study on the transition to geostrophic turbulence, and the detailed behaviour within the turbulence regime, in a rotating, laterally heated annulus of fluid. Both spatial and temporal characteristics are examined, and the results are presented in the form of wavenumber and frequency spectra as a function of a single external parameter, the rotation rate.

The transition to turbulence proceeds in a sequence of steps from azimuthally symmetric (no waves present) to chaotic flow. The sequence includes doubly periodic flow (amplitude vacillation), semiperiodic flow (structural vacillation), and a transition zone where the characteristics undergo a gradual change to chaotic behaviour. The spectra in the transition zone are characterized by a gradual merging of the background signal with the spectral peaks defining regular wave flow as the rotation rate is increased.

Within the geostrophic turbulence regime, the wavenumber spectra are characterized by a broad peak at the baroclinic scale and a power dependence of energy density on wavenumber at the high-wavenumber end of the spectrum. Our data reveal a significant dependence of the slope on the thermal Rossby number, ranging from -4.8 at $Ro_T = 0.17$ to -2.4 at $Ro_T = 0.02$. The frequency spectra also show a power dependence of the energy density on frequency at the high-frequency end of the spectrum. We find a nominal -4 power which does not appear to be sensitive to changes in Rossby or Taylor number.

1. Introduction

Interest in the behaviour of a rotating differentially heated annulus of fluid stems primarily from the nature and application of the instability that occurs there. Under appropriate conditions of lateral heating and rotation, the interior fluid density and pressure surfaces are oriented such that the potential energy in the density field can be converted into kinetic energy. The resulting flow instability is called baroclinic instability. This is the fundamental instability mechanism of large-scale midlatitude atmospheric and oceanic circulations. The widest application of the 'annulus' problem has been in atmospheric science, and has included analytical and numerical studies as well as experimental investigations. A comprehensive review of annulus flows can be found in Hide & Mason (1975).

Another aspect of the annulus problem that is of particular current interest concerns the properties of the flow field as the system is taken into turbulence through the systematic variation of an external control parameter. The process of transition to turbulence is a fundamental one which has received considerable attention

† Geophysical Fluid Dynamics Institute.
‡ Geophysical Fluid Dynamics Institute and Department of Meteorology.

recently, particularly with respect to bifurcation theory applied to dynamical systems and its relationship to the behaviour of real physical systems. In fluid dynamics this work has concentrated primarily on three broad classes: (1) Couette flow between concentric cylinders; (2) Bénard convection in a horizontal layer heated from below; and (3) shear flow, most notably the boundary layer and the free shear layer. In this context the annulus problem bears closer resemblance to the first two classes than to the third.

The present work is part of a continuing series of experimental studies of baroclinic waves in a rotating differentially heated annulus of fluid. We have previously reported on different modes of behaviour at several points in parameter space (Pfeffer, Buzyna & Kung 1980*a*) and on relationships among eddy fluxes of heat, eddy-temperature variances and basic-state temperature parameters (Pfeffer, Buzyna & Kung 1980*b*). In the present paper we consider the same series of experiments, but we concentrate on the process of transition to geostrophic turbulence and on the detailed behaviour within the turbulent regime. We examine, in particular, spatial and temporal characteristics of the temperature fields and present the results in the form of zonal wavenumber and frequency spectra as a function of a single external parameter, the rotation rate. The examination of other aspects of these flow fields (e.g. potential vorticity, enstrophy cascades and energetics) will be left to later studies. When experiments are performed at successively higher rotation rates at the same imposed horizontal temperature contrast, the flow regimes observed in sequence are (1) axisymmetric, or zonal, flow; (2) well-defined azimuthal waves with periodic time dependence (amplitude vacillation); (3) increasingly more complicated waves with semiperiodic time dependence (structural vacillation); and (4) spatially and temporally irregular, chaotic flow (geostrophic turbulence).

Spectral characteristics of baroclinic waves in an annulus have also been investigated by Rao & Ketchum (1975, 1976). Although their series of experiments spanned a broad range of parameter space, including symmetric, steady, vacillating and turbulent flows, there were too few experiments in the region between vacillating and turbulent flows to describe the spectral details of the transition process. In addition, their series of experiments did not include the time-dependent phenomenon of wave-amplitude vacillation. Their data consisted of temperature records at several locations in the fluid. Although these records were of sufficient length and high sampling frequency, the spectra were calculated from block-averaged data which resulted in considerably lower effective frequency resolution. In general, a higher-frequency resolution is desired for spectral studies of transition to turbulence (see e.g. Fenstermacher, Swinney & Gollub 1979; Gollub & Benson 1980). In our study we have a considerably higher-frequency resolution and a much greater range of frequencies. Moreover, our large temperature-measuring network permits direct determination of the spatial structure of the fluid flow field, even in turbulent flow. Accordingly, we have calculated frequency spectra at selected radii and height. We have also calculated frequency spectra of the *amplitudes* of individual zonal wavenumbers. These different forms of analysis emphasize different characteristics of the fluid behaviour. The number of experiments performed, and their distribution in parameter space, is such that they cover a broad range of behaviour and define more precisely the existence and properties of the transition zone between the regular and turbulent wave regimes. Combined temporal and spatial characteristics for this transition region have not been reported previously.

Geostrophic turbulence is, in itself, of considerable geophysical interest, and has been the subject of observational, analytical and numerical investigations. Although

some laboratory experimental work has also been conducted illustrating the nature of geostrophic turbulence at a few points in dimensionless-parameter space (Hide, Mason & Plumb 1977; Pfeffer *et al.* 1980*a*), there have been no previous comprehensive studies of both the spatial and temporal properties of the fluid behaviour over a broad range of imposed temperature contrasts and rotation rates for a given fluid and container geometry. This paper includes the results of such a comprehensive study.

2. Experimental details

2.1. *Experimental apparatus and procedures*

For the purposes of the present study, we utilized data from two series of experiments (designated as the C- and D-series), which are described in detail by Pfeffer *et al.* (1980*a*, *b*). Here we present only a general outline of the apparatus and procedures with details pertinent to this investigation.

The experiments were conducted in an annular chamber formed by two coaxial brass cylinders imbedded in, and normal to, a flat horizontal Plexiglas base. The inner and outer radii of the annular chamber were 30.48 ± 0.01 cm and 60.96 ± 0.01 cm respectively. The working fluid, 1.52 cs silicone fluid (Prandtl number $Pr = 21$), was placed into the annular region to a depth H of 15.00 ± 0.05 cm. The top surface was left free, and the annular chamber was covered to eliminate interaction with the ambient air. A horizontal temperature contrast was imposed across the annulus gap by means of thermostatically controlled baths in contact with the outside of the outer cylinder and the inside of the inner cylinder forming the annular chamber. The inner and outer cylindrical walls were maintained at cold and warm temperatures respectively. Several imposed temperature contrasts were used, from 2.5° to 20 °C. The entire annulus assembly was mounted on a turntable such that the axis of symmetry of the annulus coincided with the axis of rotation of the turntable. The rotation rate was varied from 0.35 to 1.57 rad/s. Each experiment was begun by establishing the desired imposed horizontal temperature difference with the turntable at rest and then bringing the turntable quickly to the desired rotation rate. This is referred to as a 'sudden-start' procedure.

The temperature field in the fluid interior was measured with a staggered array of miniature bead thermistors (< 0.05 cm diameter) attached to 72 radially oriented frames. The frames were spaced at intervals of 5° of azimuth. In the C-series experiments, individual thermistors were located at 2016 points in the fluid, 28 in each of the 72 radial planes. The distribution of these thermistors (detailed by Pfeffer *et al.* 1980*a*) was designed to allow accurate interpolation of the temperature data to locations of desired height and radius within most of the volume. For the purpose of estimating zonal wavenumber spectra, we utilized 72 equally spaced temperatures along circles of radii 37.14 and 47.31 cm from the rotational axis (respectively 0.22 and 0.55 of the annulus gap width measured from the inner cylinder) at mid-depth. All of these temperatures were interpolated from thermistor measurements at other locations. Interpolated data were also used to construct synoptic temperature fields at mid-depth. For the purpose of estimating frequency spectra at individual points in the fluid, we used 9 individual thermistor readings, evenly spaced along the same two circles at a height of 6 cm.

The D-series contained individual thermistors at 936 locations, and groupings of four thermistors (with perimeters of approximately 0.15 cm diameter in the horizontal plane) at 360 other locations (as detailed by Pfeffer *et al.* 1980*b*). These groupings formed thermistor anemometers called 'quadruples'. For the purpose of estimating

time-averaged zonal wavenumber spectra in geostrophic turbulence, we used only the temperature data in the D-series derived from 72 evenly-spaced thermistors located on a circle at mid-depth and 43.82 cm radius (0.44 of the gap width). Experimental data in both series were recorded with a 2048-channel, computer-controlled, digital data-acquisition system with a constant scan rate of 20000 channels/s.

Temperature data were recorded either once or twice every rotation in the C-series and once every three to five rotations in the D-series, beginning from two to four hours (1000–4000 rotations) after the start of each experiment and extending for approximately three hours ($\sim$ 1300–3000 rotations, depending upon the rotation rate). Based upon temperature records taken from the start of rotation, we found that the fluid behaviour in the annulus was well established in approximately half an hour. The additional time allowed before gathering data ensured that the flow was in a stationary state relative to the constant externally imposed temperature contrast and rotation rate.

The raw data consisted of a time sequence of out-of-balance bridge voltages, which were converted into a time sequence of temperature measurements by means of calibration experiments. At each time, all thermistor readings were scanned and recorded within 0.1 s. The r.m.s. uncertainty of the temperature measurements, determined from the calibration results, was ± 0.005 °C.

2.2. *Analysis of experimental data*

The C-series experiments provided high resolution (sampling frequency) and long time records, with up to 3000 time samples of temperature at each thermistor location in the case of the turbulence experiments. The data records corresponding to each of the nine thermistor locations at radii 37.14 and 47.31 cm and height 6 cm were subjected to frequency spectrum analysis. The power-spectral density (p.s.d.) of the temperature was estimated from the squared modulus of a fast Fourier transform and expressed in terms of °C^2 per unit frequency, with frequencies expressed in cycles per rotation. Since sampling in the C-series experiments was done once or twice every rotation, the maximum (or Nyquist) frequency was respectively 0.5 or 1.0 cycles per rotation. The minimum frequency depended on the record length and was typically between 10^{-3} and 10^{-4} cycles per rotation.

In order to obtain sharp and distinct peaks and reduce statistical noise in the spectra, we utilized two data-treatment methods, one on the source data and one on the Fourier transform. The number of data points in the temperature records was 'tuned' by progressively shortening the record length and observing the spectra. The record length selected was the one that gave the most distinct peaks. This procedure reduced end effects on the dominant features of the spectra; it proved very effective in periodic and semiperiodic records and of no particular consequence in the turbulence records. The raw spectra obtained in this way represent behaviour at a single location. Note, however, that at each radius and depth in the fluid there are nine equally spaced thermistor locations. None of these locations is preferred over any other; they all exhibit essentially the same behaviour and differ from each other only with respect to phase and statistical noise. The effect of statistical noise can therefore be reduced by averaging the raw spectra obtained from each of the nine locations at the same radius and height. The spectrum obtained by such averaging is representative of the raw spectra at each of the individual locations, but with a reduced noise level and sharper peaks. No significant peaks were added or eliminated by this procedure. This average spectrum will therefore be used throughout the present paper to represent the spectrum at a single radius and height.

In the turbulence regime some additional smoothing of the spectra was also desirable. This was accomplished by hanning, an operation which consists of taking a running average of the power spectral densities at three adjacent points with the weights $\frac{1}{4}$, $\frac{1}{2}$ and $\frac{1}{4}$. Hanning was done twice, which is equivalent to a single pass of a five-point running average with the weights $\frac{1}{16}$, $\frac{1}{4}$, $\frac{3}{8}$, $\frac{1}{4}$ and $\frac{1}{16}$.

In both the C- and D-series experiments, wavenumber spectra with resolution up to wavenumber 36 were estimated from the squared modulus of a fast Fourier transform of the 72 temperature values on each circle. As noted earlier, the data used for this purpose were interpolated in the C-series and measured directly in the D-series. Such spectra were calculated for all scans of the data network and linearly averaged to obtain the characteristic time-mean wavenumber spectrum corresponding to each experiment. In the C-series we also calculated the frequency spectra of the *wave amplitudes* using the same procedures as in the frequency analyses of the temperature records at individual points in the fluid. This included two passes of hanning in the case of structural vacillation and geostrophic turbulence. In the D-series the sampling frequency was lower than that in the C-series, and the number of data records was comparatively small. This series was therefore used only to estimate time-averaged wavenumber spectra which we evaluated only in the geostrophic turbulence regime.

3. Experimental results

The flow in the rotating annulus has generally been categorized into three broad regimes: the symmetric, the regular-wave and geostrophic-turbulence (irregular-wave) regimes. Each regime, in turn, may have more than one behavioural state. Of particular interest here is the sequence of flows encountered as the system is taken progressively from the symmetric through the regular-wave regime into geostrophic turbulence. Such a sequence is illustrated by the C-series of experiments listed in table 1 and shown along the diagonal line in figure 1, at fixed imposed temperature contrast $\Delta T = 10$ °C and successively larger rotation rates Ω. Next to each point in the figure is the experiment number, in parentheses, and the observed dominant zonal wavenumber.

Characteristic horizontal temperature fields at mid-depth in the fluid, corresponding to each of these experiments, are shown in figure 2. These fields were constructed by interpolation from the vast thermistor network suspended in the fluid interior. The isotherms are drawn in increments of 0.2 °C and the sequence is arranged from left to right in order of increasing rotation rate starting in the upper left-hand corner.

At a given ΔT and relatively small Ω (not shown in figure 2) the flow is axially symmetric. At somewhat larger Ω transition to the regular-wave regime occurs. Departures from zonal symmetry, which are extremely small in experiment C26, increase in magnitude with Ω through to experiment C28, after which they take on increasingly more complicated spatial configurations, culminating in highly irregular patterns at the largest rotation rates. We categorize the regular-wave regime as spanning all experiments C26–C78 inclusive.

Within the regular-wave regime, two distinct time-dependent states are found, separated by a sharp boundary in dimensionless parameter space. These are *amplitude vacillation* at lower Ω and *structural vacillation* at higher Ω. Amplitude vacillation is characterized by large, periodic growth and decay of the energy of the wave field (Pfeffer, Buzyna & Fowlis 1974; Pfeffer *et al.* 1980*a*). In figure 2 the temperature fields in the amplitude-vacillation experiments (C75 and C28) are shown at times approximately midway between the maximum and minimum wave amplitude.

Experiment	ΔT (°C)	Ω (s^{-1})	Ro_T	Ta (10^8)	Number of data points
26	10	0.349	1.74	1.07	—
75	10	0.384	1.44	1.30	1396‡
28	10	0.436	1.11	1.67	1338‡
76	10	0.489	0.888	2.09	910‡
29	10	0.524	0.773	2.41	1296‡
83	10	0.576	0.639	2.91	2140‡
77	10	0.628	0.537	3.46	2100‡
82	10	0.698	0.435	4.28	1562
78	10	0.785	0.344	5.40	2212‡
32	10	0.873	0.278	6.67	1852
31	10	0.960	0.230	8.07	1620
72	10	1.047	0.193	9.61	2334
79	10	1.257	0.134	13.8	2848
80	10	1.396	0.109	17.0	2388
81	10	1.571	0.086	21.6	2892
97	20	1.571	0.172	21.6	2882
42	5	1.571	0.040†	16.5†	2724

† Fluid depth 14 cm instead of 15 cm.
‡ Sampling frequency of twice per rotation (all others once per rotation).

TABLE 1. Experimental parameters for C-series experiments

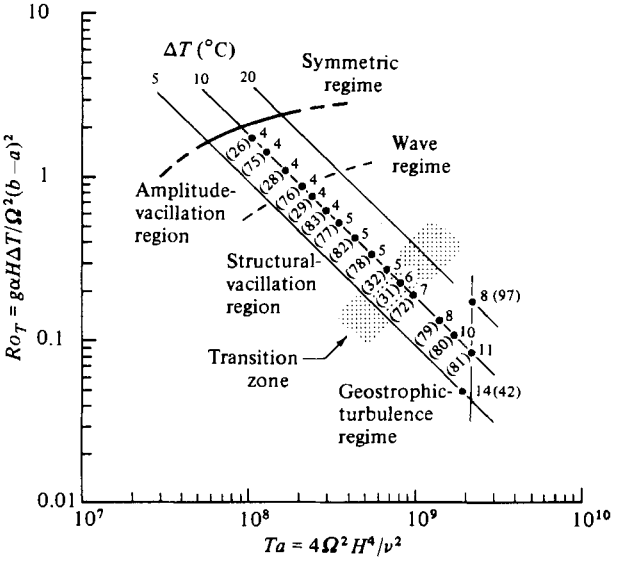

FIGURE 1. Regime diagram, Rossby number Ro_T versus Taylor number Ta at Prandtl number $Pr = 21$, for experimental series C. The observed dominant zonal wavenumber and the experiment number (in parentheses) are shown next to each point. Dimensionless parameters Ro_T and Ta are defined on the coordinate axes (g is the acceleration due to gravity, α and ν are respectively the coefficients of volume expansion and kinematic viscosity, a and b are respectively the inner and outer radii of the annulus, H is the fluid depth, Ω is the rate of rotation of the annulus and ΔT is the imposed temperature contrast). Note that experiment C42 is at the same Ω as C81 and C97; the Taylor number is lower owing to lower fluid depth (14 cm instead of 15 cm) in this experiment.

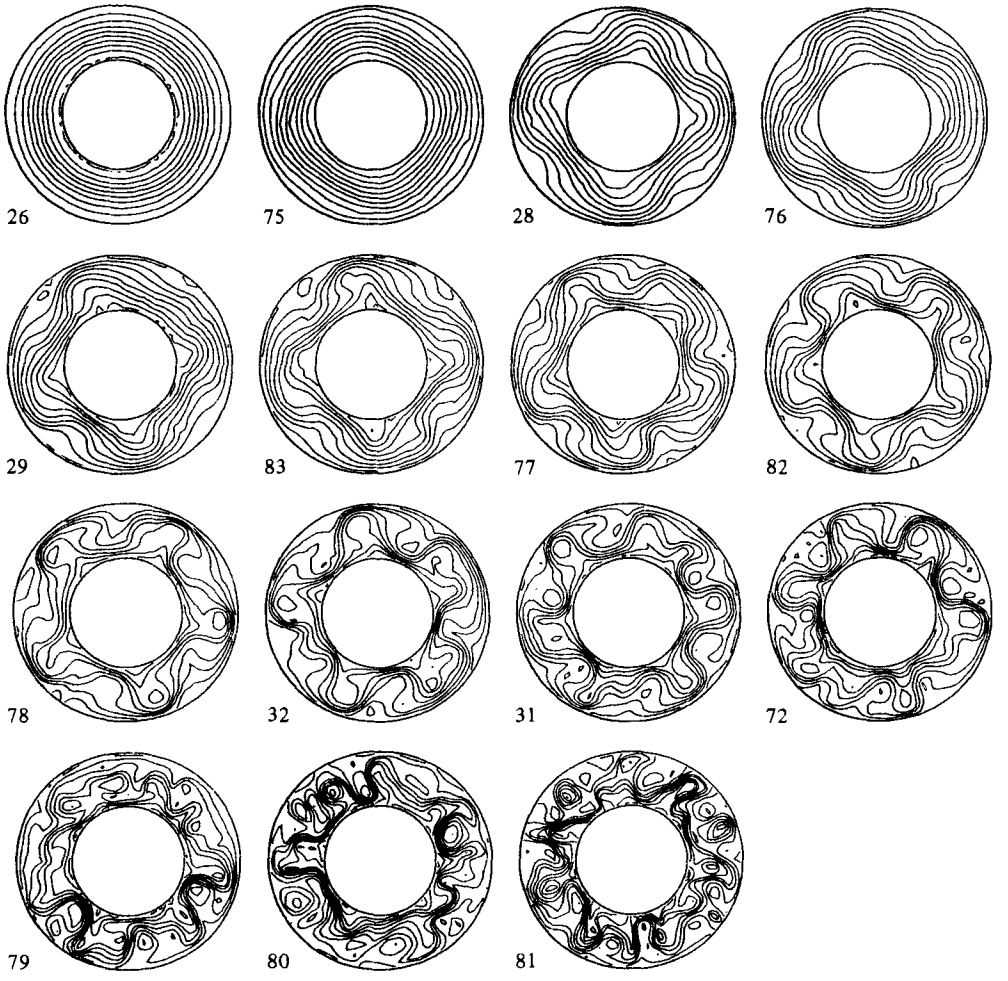

FIGURE 2. Characteristic horizontal temperature fields at mid-depth in the fluid corresponding to each of the experiments shown in figure 1 at $\Delta T = 10$ °C. The number in the lower left of each circle represents the experiment number. The isotherms are drawn in increments of 0.2 °C and the sequence is arranged from left to right in order of successively larger rotation rates, starting in the upper left-hand corner.

Structural vacillation (experiments C76–C78) is characterized by fluctuations which take place mainly in the wave shape and in the *radial distribution* of the wave energy, with comparatively small variations in the total energy of the wave field. These fluctuations are of higher frequency than those of amplitude vacillation, and are semiperiodic and irregularly modulated over long periods of time (Pfeffer *et al.* 1980*a*).

At relatively large rotation rates (experiments C79–C81) the temperature and flow patterns are found to be highly irregular in space and chaotic in time. We refer to this behaviour as geostrophic turbulence, a particular type of turbulence which is characteristic of stratified fluids in quasi-geostrophic, quasi-hydrostatic and quasi-non-divergent balance (Rhines 1979). Between the wave and geostrophic-turbulence regimes (experiments C32, C31 and C72) the temperature and flow patterns display characteristics of both regimes. We regard this region of dimensionless-parameter space, indicated by the stippled band in figure 1, as the transition zone.

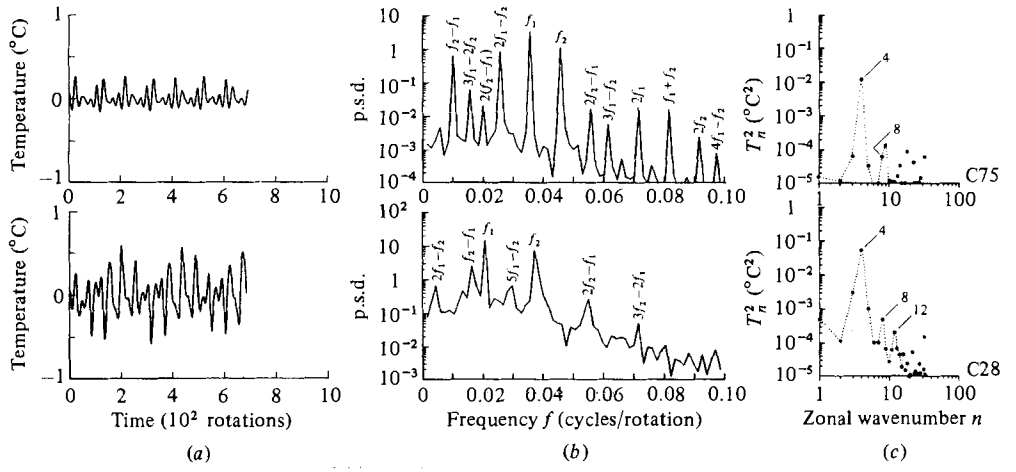

FIGURE 3. Characteristics of the amplitude-vacillation region: (*a*) time records of temperature departures from the mean at a single location near mid-depth and mid-gap; (*b*) frequency spectra of the temperature records (p.s.d. is in °C^2 per unit frequency); (*c*) time-averaged zonal-wavenumber spectra obtained from interpolated temperature data at mid-depth and the same radius as the time records in (*a*).

We present our experimental results in several sections below, in a sequence of natural groupings according to common dominant characteristics en route to turbulence: amplitude vacillation (§3.1), structural vacillation (§3.2), transition zone (§3.3) and the geostrophic-turbulence regime (§3.4). In the last section we examine the characteristics of geostrophic turbulence over a relatively broad range of parameters, at several imposed temperature contrasts and rotation rates in the C-series experiments, and we present additional results from experimental series D.

An analysis of the first experiment in the sequence, C26, will not be presented here. The wave signal in this experiment was too weak, and too close to the noise level, to give reliable temporal characteristics. The time-averaged zonal-wavenumber spectrum, however, revealed the presence of zonal wavenumber 4. This information is barely detectable in the temperature field in figure 2, and the flow appears nearly axisymmetric. This experiment is close to the boundary between the symmetric and wave regimes, as shown in figure 1.

3.1. *Amplitude-vacillation region*

The characteristics of amplitude vacillation are summarized in figure 3. Figure 3(*a*) shows time records of temperature departures from time mean at a point near mid-depth ($0.4H$) and midgap (0.55 of the annulus gap width measured from the inner cylinder) in experiments C75 and C28. Figure 3(*b*) shows frequency spectra in the frequency range $0 < f < 0.1$ cycles per rotation, derived from these records. The higher-frequency portion of the spectrum is omitted because the power density above $f = 0.1$ cycles per rotation is negligible. Figure 3(*c*) shows time-averaged wavenumber spectra obtained from the interpolated temperature data at the 72 evenly spaced gridpoints at mid-depth and the same radius as the time records in figure 3(*a*). For consistency with other papers in the literature, the frequency and wavenumber spectra are plotted on log–linear and log–log scales respectively.

Figure 3 reveals that amplitude vacillation is characterized by a strongly modulated, periodic temperature–time signal, a single dominant azimuthal wavenumber with

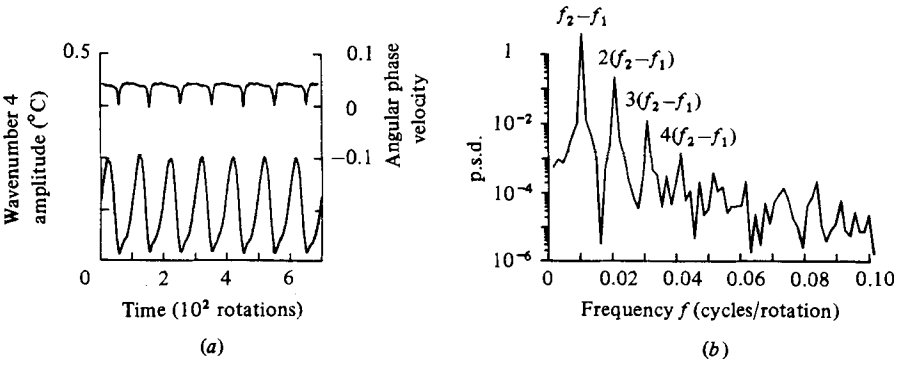

FIGURE 4. Temporal characteristics of dominant zonal wavenumber 4 in amplitude-vacillation experiment C75: (*a*) amplitude and angular phase velocity are shown as functions of time in the lower and upper portions of the figure respectively (angular phase velocity is in cycles per rotation, with positive values indicating counterclockwise motion relative to the annulus); (*b*) frequency spectrum of the wave amplitude (p.s.d. is in °C² per unit frequency).

weak sidebands and higher harmonics, and two incommensurate frequencies (f_1 and f_2) with weaker linear combinations of these frequencies. In experiment C75 the sidebands (wavenumbers 3 and 5) and the first higher harmonic (wavenumber 8) are very weak and of comparable magnitude. The peak at wavenumber 9 is not a characteristic of the temperature field, but is due to interpolation errors associated with the particular distribution of thermistor probes, as discussed by Pfeffer *et al.* (1980*a*). Such errors do not produce a noticeable spectral peak in other experiments in which the signal is stronger. In experiment C28 the magnitude of the side bands is larger than that of the higher harmonics. This is a common configuration in amplitude vacillation.

The most prominent characteristic of amplitude vacillation is the periodic time dependence of the dominant wave amplitude and phase velocity (Pfeffer *et al.* 1974). We illustrate this characteristic in figure 4(*a*), where the amplitude and angular phase velocity of wavenumber 4 in experiment C75 are shown as functions of time in the lower and upper portions of the diagram respectively. The characteristic frequency of the vacillation is clearly evident in these records. This frequency, which is equal to the difference of the two incommensurate dominant frequencies in the spectrum of the temperature record at a single location in the fluid (viz f_2-f_1), is the dominant one in the frequency spectrum of the amplitude of wavenumber 4 shown in figure 4(*b*). The other peaks in the spectrum with successively lower magnitudes correspond to successively higher harmonics of this frequency. The side bands and the higher harmonics of wavenumber 4 in the wavenumber spectrum have frequency spectra similar to that of figure 4(*b*).

The time-averaged angular phase velocity (figure 4*a*), expressed in waves, or cycles, per rotation, is numerically equal to f_1. This frequency is therefore clearly identifiable with the average drift of the dominant wavenumber. It is, in general, incommensurate with the amplitude vacillation frequency f_2-f_1.†

† The choice of f_1 and f_2 as the fundamental frequencies, based on the fact that these were the dominant frequencies in figure 3(*b*), is somewhat arbitrary. We could equally well have selected the drift frequency f_1 and the vacillation frequency f_2-f_1 as the two fundamental frequencies describing amplitude vacillation. Alternatively, recognizing that f_1 represents the drift frequency, one could also make a Galilean transformation and thereby interpret the phenomena as singly periodic flow with frequency f_2-f_1 in the new reference frame.

To a first approximation, f_1 and f_2 can be interpreted as being associated with the *constant* angular drift of *two* wave patterns with the *same* zonal wavenumber but with *different* phase speeds, corresponding to the frequencies f_1 and f_2. The amplitudes of these two zonal waves are constant and unequal. It can be readily shown that the passage of two such zonal waves relative to each other will result in constructive and destructive interference and a combined waveform whose amplitude and phase speed oscillate with the frequency f_2-f_1, and whose mean phase speed corresponds to f_1, the larger of the two peaks. The possibility for the existence of such waves has been shown theoretically by Lindzen, Farrell & Jacqmin (1982) and Moroz & Brindley (1982), although we do not agree with the interpretation of our experimental data by Lindzen *et al.*

3.2. *Structural-vacillation region*

According to Pfeffer *et al.* (1980*a*), structural vacillation is characterized by a semiperiodic oscillation of the wave energy-centres in the radial direction. In order to optimize the signal characterizing this time dependence, we used the temperature data near one-quarter (0.22) gap width, measured from the inner wall. The temperature records at this radius and at height $0.4H$ corresponding to the six experiments exhibiting structural vacillation are shown in figure 5(*a*). In contrast with the strongly modulated signals in amplitude vacillation, these records display rather uniform periodic behaviour with only a very weak low-frequency modulation and a gradual emergence of a high-frequency oscillation superimposed on the regular periodic signal with increased rotation rate. The frequency spectra of the individual temperature records (figure 5*b*) are characterized by a single dominant frequency f_1 and its two, lower-amplitude, higher harmonics $2f_1$ and $3f_1$. The frequency f_s designated by the dashed vertical line in the figure will be discussed later in this section. With increased rotation rate, the frequencies of the three dominant modes become progressively lower, the power density in the higher harmonics increases relative to that in the fundamental frequency, and the background signal increases relative to that of the three dominant frequencies. The zonal-wavenumber spectra (figure 5*c*) estimated from interpolated data at the same radius, but at mid-depth, are characterized by a dominant mode and its two, lower-amplitude, higher harmonics. With increased rotation rate, the variance in the higher harmonics increases with respect to that in the dominant mode and, with the exception of experiment C76, the background signal is observed to increase relative to that of the three dominant zonal harmonics.

Experiment C76 was somewhat unique in that it exhibited characteristics first of amplitude vacillation and later of structural vacillation. No changes in external parameters occurred during this experiment, and data recording began after the usual period of time allowed for the elimination of transient effects. The cause of this behaviour is not clear, although it appears that relaxation of a given flow to its non-transient state near points of bifurcation takes more time than it would away from such points, well within its own domain. The first portion of the data record exhibiting amplitude vacillation was too short for adequate analysis and was thus excluded. The record and the analyses shown, begin with the 400th rotation, after which the flow appeared to have settled into its new order. As a consequence of this behaviour, we interpret the change between amplitude and structural vacillation to occur relatively abruptly in dimensionless-parameter space, and we represent the boundary between them in figure 1 by the dashed line through experiment C76. The frequency resolution in this experiment is relatively coarse owing to the short record

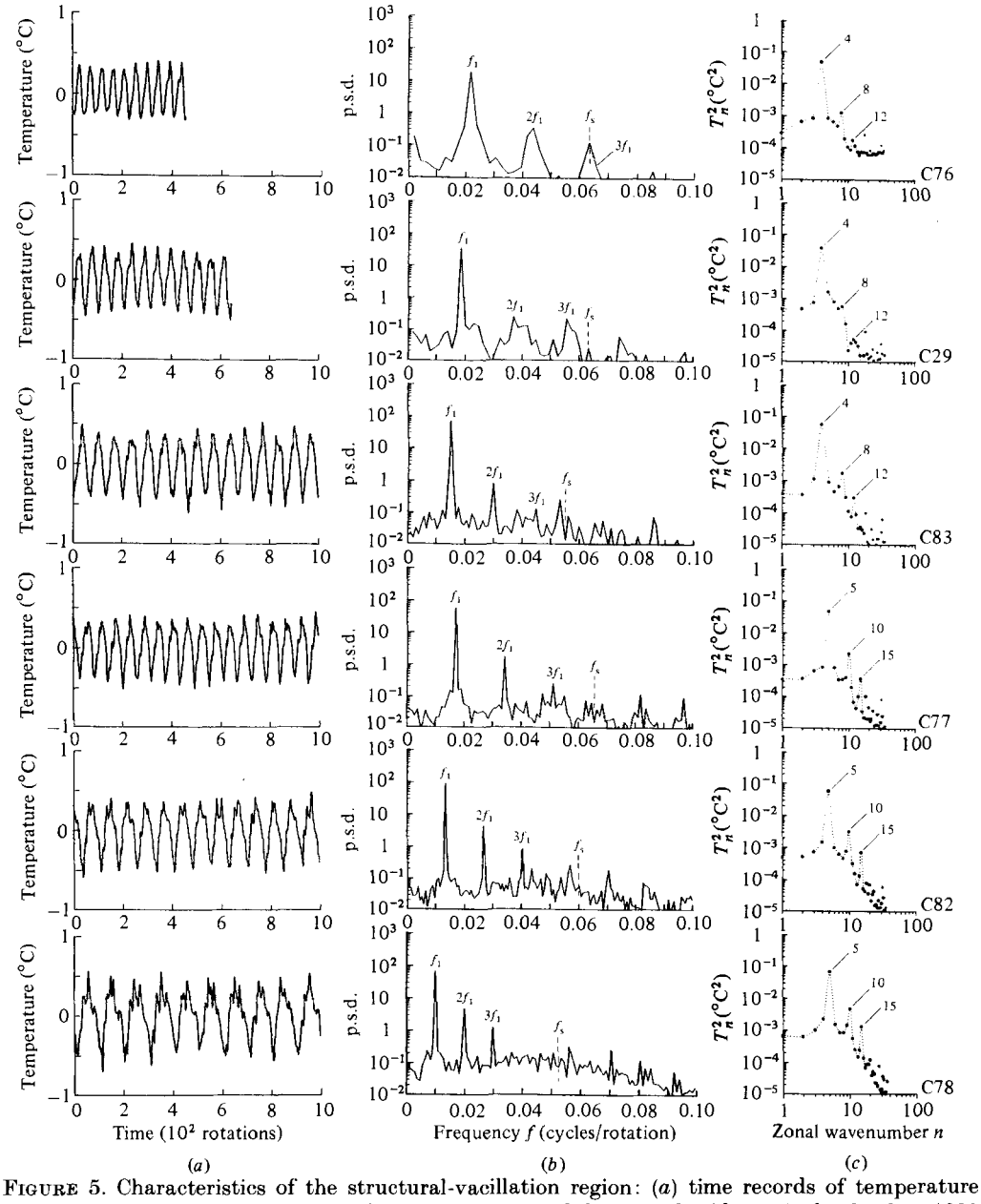

FIGURE 5. Characteristics of the structural-vacillation region: (*a*) time records of temperature departures from the mean at a single location near mid-depth and mid-gap (only the first 1000 rotations are shown in experiments C83, 77, 82 and 78); (*b*) frequency spectra of the temperature records (p.s.d. is in °C² per unit frequency); (*c*) time-averaged zonal-wavenumber spectra obtained from interpolated temperature data at mid-depth and the same radius as the time records in (*a*).

length. The flattened tail-end of the wavenumber spectrum, past wavenumber 12, figure 5(*c*), is due to a faulty thermistor in one of the locations near the cold wall.

From the time records and spectra in figure 5, and from sequences of synoptic temperature charts (not shown here), we can infer that the dominant frequency and its higher harmonics are associated with the counterclockwise drift of the dominant zonal wavenumber and its higher harmonics. This drift velocity decreases with

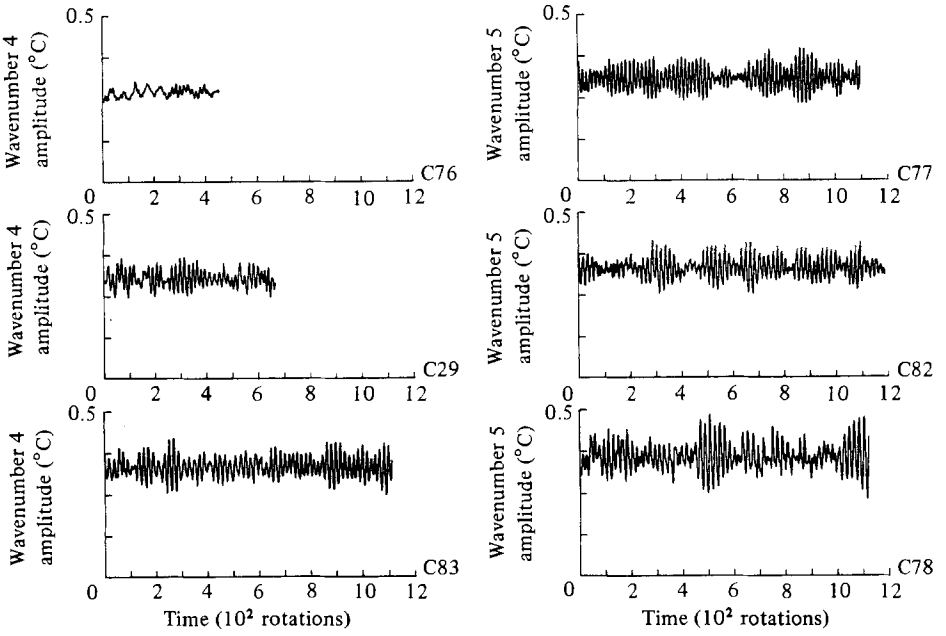

FIGURE 6. Time variations of the dominant zonal wave amplitude for each of the structural vacillation experiments. The sequence is arranged in two columns in order of increasing rotation rate starting in the upper left-hand corner.

increased rotation rate, accounting for the progressively lower values of these frequencies from the upper to the lower part of the figure. The progressively increased strength of the higher harmonics and background signals in both the wavenumber and frequency spectra are believed to be due to the broadening of the range of baroclinic instability (see Pfeffer *et al.* 1980*b*, figure 16) and to increased nonlinearity with increased rotation rate.

Apparently, the frequency spectra of the temperature records at a single location in the fluid have not revealed any significant information concerning the characteristic time-dependent behaviour we call structural vacillation, namely the semiperiodic, or intermittent, oscillation of the wave-energy centres in the radial direction. This characteristic time dependence is, however, exhibited clearly in the time records of the zonal wave amplitudes shown in figure 6. These records reveal closely spaced bursts of sustained oscillations increasing in amplitude with rotation rate. Similar behaviour (not shown here) is observed at other radii in the annular region. The records on either side of mid-radius, however, are approximately out of phase with each other and reflect the primarily spatial nature of this oscillation (for more details see Pfeffer *et al.* 1980*a*). From the number of cycles observed over the length of these amplitude–time records, we can obtain an approximate value for the frequency of the structural-vacillation phenomenon. This frequency f_s is a mean value over the length of the record and is within 10 % of the frequency measured over short portions of the record with clearly sustained oscillations. A more quantitative measure of f_s can be obtained from a spectral analysis of the time records of the zonal wave amplitudes. The results of such an analysis in the case of experiment C78 are presented in figure 7(*b*). Here, we see frequency spectra of the amplitudes of the dominant zonal wavenumber, 5, and its higher harmonics, 10 and 15. These spectra have been smoothed by two passes of hanning. The time records of the amplitudes

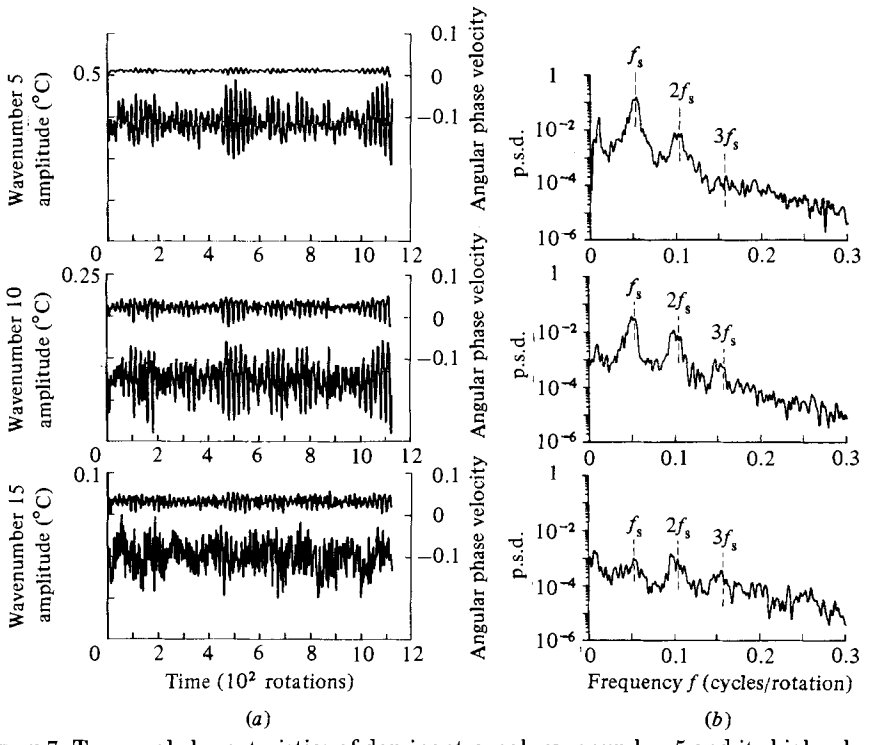

FIGURE 7. Temporal characteristics of dominant zonal wavenumber 5 and its higher harmonics 10 and 15 in structural-vacillation experiment C78: (*a*) amplitudes and angular phase velocities as functions of time are shown in the lower and upper portions of the figure respectively (angular phase velocity is in cycles per rotation, with positive values indicating counterclockwise motion relative to the annulus); (*b*) frequency spectra of the wave amplitudes (p.s.d. is in °C² per unit frequency).

and angular phase speeds of these waves are shown in figure 7(*a*), opposite the corresponding frequency analyses. The semiperiodic oscillations of the phase speeds are seen to be in harmony with those of the amplitudes. The average values of the angular phase speeds of wavenumbers 5, 10 and 15, expressed in units of cycles per rotation, are numerically equal to the frequencies f_1, $2f_1$ and $3f_1$ respectively.

The frequency spectrum of zonal wavenumber 5 is dominated by a broad peak centred approximately at f_s, with weaker peaks at $2f_s$ and at f_1. The peaks at f_s and $2f_s$ are relatively wide in comparison with the sharp peak defining the frequency f_1 in figure 5. For example, 14 frequencies (between 0.046 and 0.059) in the peak centred at f_s contain 69 % of the total variance, nine of which have comparable magnitudes. In contrast, the single frequency f_1 possesses approximately 80 % of the total variance in the spectra of the temperature records at a single location. The relative broad peak around f_s reflects the particular semiperiodic nature of the structural vacillation phenomenon in these experiments.

The time variations of the amplitude and angular phase velocity of wavenumber 10 (figure 7*a*) are roughly similar to those of wavenumber 5. The magnitude of the oscillations in the phase velocity are, however, larger, and the frequency spectrum of the wave amplitude (figure 7*b*) contains a substantially larger peak near $2f_s$ and an additional comparatively small peak near $3f_s$. Wavenumber 15 is relatively weak, with considerable background noise superimposed on the time variations of its amplitude and phase velocity. Its frequency spectrum is dominated by a peak near

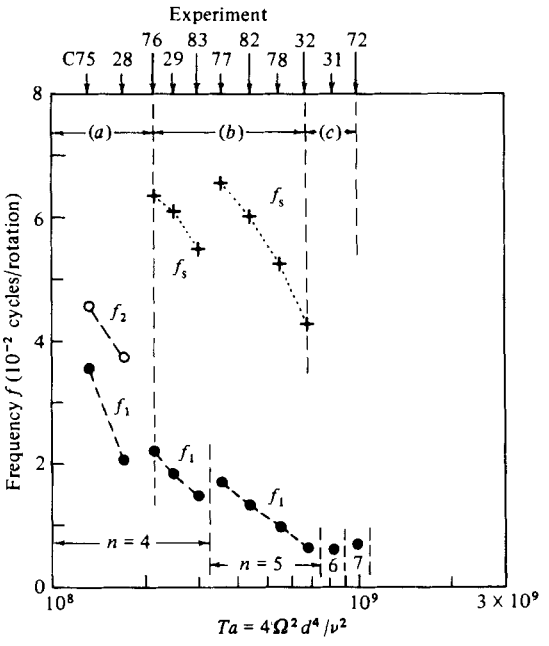

FIGURE 8. Variation of the fundamental frequencies f_1 and f_2 in the amplitude-vacillation region (a), f_1 and f_s in the structural vacillation region (b), and f_1 in the transition zone (c), as a function of Taylor number at $\Delta T = 10$ °C.

$2f_s$, with comparable peaks near f_s and $3f_s$ and a comparatively high level of broadband background noise.

The general characteristics of the other experiments in the structural vacillation sequence are similar to those in the above example, particularly with respect to the nature and composition of the relatively broad major peak in the frequency spectrum of the dominant zonal wavenumber. Over the length of the experimental record, the characteristic structural vacillation frequency f_s, is thus represented by a band or range of frequencies rather than a sharp peak such as is characteristic of the frequency f_1.

The variations of the fundamental frequencies f_1 and f_s as functions of the rotation rate (expressed by the Taylor number) are shown in figure 8. Also included in this figure is the amplitude-vacillation region, with frequencies f_1 and f_2 shown, and the transition zone, which will be discussed in §3.3. A characteristic and dominant feature of the drift frequency f_1 (solid circles), is a general decrease in frequency with increased rotation rate, from the amplitude vacillation through the transition regions. Note the implied discontinuities in f_1 accompanying wavenumber changes in the flow field. There is also an implied discontinuity between the amplitude and structural vacillation regions. In the amplitude-vacillation region the second fundamental frequency f_2 (open circles) also decreases with increased rotation rate, and the difference $f_2 - f_1$, the vacillation frequency, increases with increased rotation rate. The increase in the amplitude-vacillation frequency agrees with the observations of the vacillation period of other investigators (Fowlis & Pfeffer 1969; White & Koschmieder 1981; Hignett 1982 personal communication).

The structural vacillation frequency f_s (crosses, figure 8) also exhibits a downward trend with increased rotation rate and a discontinuity at a wavenumber change.

The results of figure 8 would seem to suggest that structural vacillation may also be regarded as a doubly periodic phenomenon, although strictly speaking f_s is not characterized by a single frequency, or a single sharp peak, as in amplitude vacillation. The characteristic oscillations occur in closely spaced bursts and give this phenomenon a semiperiodic or intermittent quality over the length of a long record. We note, however, that, during a portion of the record with sustained oscillations, f_s appears to be a well-defined frequency and the flow may appear as doubly periodic at such times.

The suggestion that structural vacillation can be visualized in terms of a doubly periodic phenomenon is not immediately apparent when one examimes the frequency spectra of temperature records at a single location (figure 5*b*). One would expect a second incommensurate characteristic frequency to be evident in the spectra, if not f_s then some other frequencies which would be related to f_s through some linear combination with f_1 (for example, peaks representing the modulation of f_1 by f_s, as in an FM radio signal). We have indicated the mean-frequency f_s by dashed vertical lines in the frequency spectra of figure 5(*b*). There is nothing at these locations, or at $f_s \pm f_1$, that might reveal the presence of the vacillation frequency, f_s. One might easily conclude, therefore, on the basis of an examination of these spectra alone, that they represent primarily singly periodic flows. The reason for the absence of one or more significant peaks associated with the structural-vacillation frequency f_s, is twofold. First, the amplitude of the radial oscillation is comparatively weak (i.e. the fluctuation of the zonal wave amplitude about its mean at a given radius is approximately 25% in experiment C78 as compared with nearly 100% in the amplitude vacillation experiments). Secondly, this oscillation is associated with a broad peak in the frequency spectrum of the dominant azimuthal wavenumber (figure 7). This spreads the signal in the frequency spectrum of the temperature record at a point over a large number of frequencies, which are thereby submerged in the background signal. As a result, the frequency spectrum at a single location is dominated entirely by the azimuthal wave drift, and it is necessary to examine the frequency spectrum of the dominant azimuthal wave amplitude to isolate the presence of the vacillation frequency.

3.3. *Transition zone*

The primary purpose of designating a transition zone (the stippled band in figure 1) is to indicate that the change from predominantly semiperiodic to predominantly turbulent behaviour occurs gradually in parameter space. This change in temporal and spatial characteristics is represented by the sequence of experiments C32, 31 and 72. The temperature records at a single location, and their frequency and zonal wavenumber spectra, are shown in figure 9. The record corresponding to experiment C32 (figure 9*a*) appears similar to that in the last experiment in §3.2 (viz C78). We still see a well-defined low-frequency oscillation with superimposed high-frequency fluctuations. The latter, however, are of higher amplitude here. The frequency spectrum (figure 9*b*) is still characterized by a dominant sharp peak at f_1, although this peak accounts for less of the total variance than in C78. The higher harmonics, $2f_1$, and especially $3f_1$, are less well-defined now. The background signal has increased substantially and has effectively submerged the peak at $3f_1$. The zonal-wavenumber spectrum (figure 9*c*) continues to be characterized by a dominant wavenumber and its higher harmonics, although here too the background signal has increased in magnitude relative to the dominant peaks.

In the next experiment in the sequence, C31, the amplitude of the high-frequency

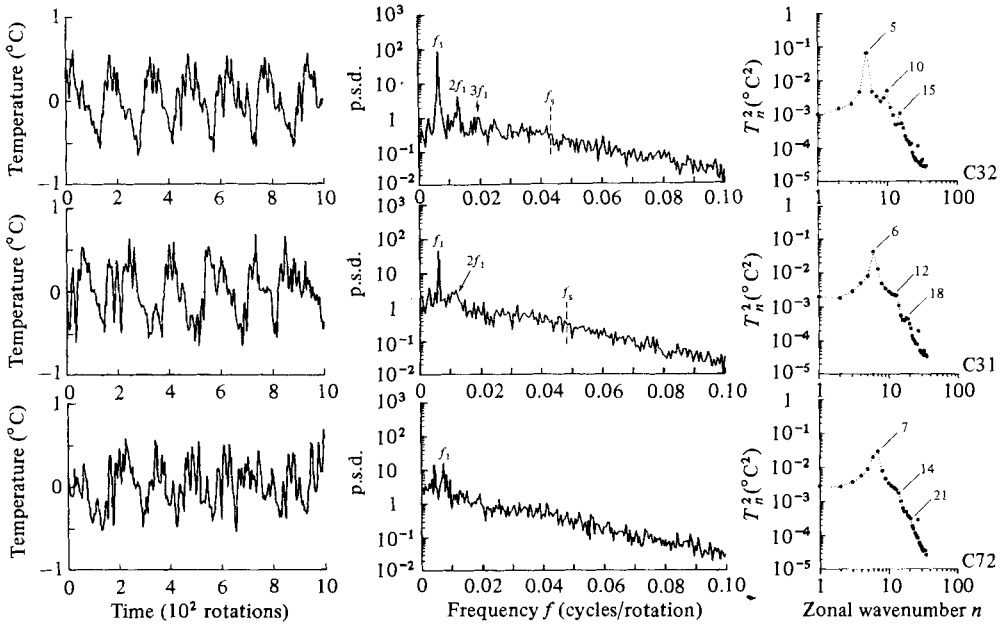

FIGURE 9. Characteristics of the transition zone: (*a*) time records of temperature departures from the mean at a single location near mid-depth and mid-gap (only the first 1000 rotations are shown here); (*b*) frequency spectra of the temperature records (p.s.d. is in °C² per unit frequency); (*c*) time-averaged zonal-wavenumber spectra obtained from interpolated temperature data at mid-depth and the same radius as the time records in (*a*).

fluctuations in the temperature record has increased further. The dominant peak f_1 is still sharp, but of lower magnitude relative to the background signal, which has now risen to the level of the higher harmonics and has effectively merged with them. The zonal-wavenumber spectrum shows a similar development in characteristics with respect to the behaviour of the higher harmonics; the background level has also risen relative to the harmonics and has nearly merged with them. This spectrum continues to be characterized by a single peak, although it now appears to be broader, as its sidebands have increased in amplitude.

In the last experiment of this sequence, C72, the amplitude of the higher-frequency fluctuations in the temperature record has increased further, and these fluctuations now begin to obscure the lower-frequency oscillation due to wave drift, which was so clearly evident in the preceding experiments. In the frequency spectrum of the temperature record we can still identify a peak, f_1, which can be related to the drift of the dominant zonal wavenumber. It is, however, no longer clearly dominant and contains only a small fraction of the total variance. The frequency spectrum at frequencies higher than 0.01 cycles per rotation is broadband with a systematic decrease in the power-spectral density with frequency. The zonal-wavenumber spectrum continues to be dominated by a single peak, although it is now relatively broad. The higher harmonics now appear as bumps on the high-wavenumber tail of the spectrum, which appears to follow a power relationship between the temperature variance and zonal wavenumber.

The transition region is represented in terms of the temporal behaviour of the dominant zonal wavenumber in figure 10. In the first experiment, C32, the phase

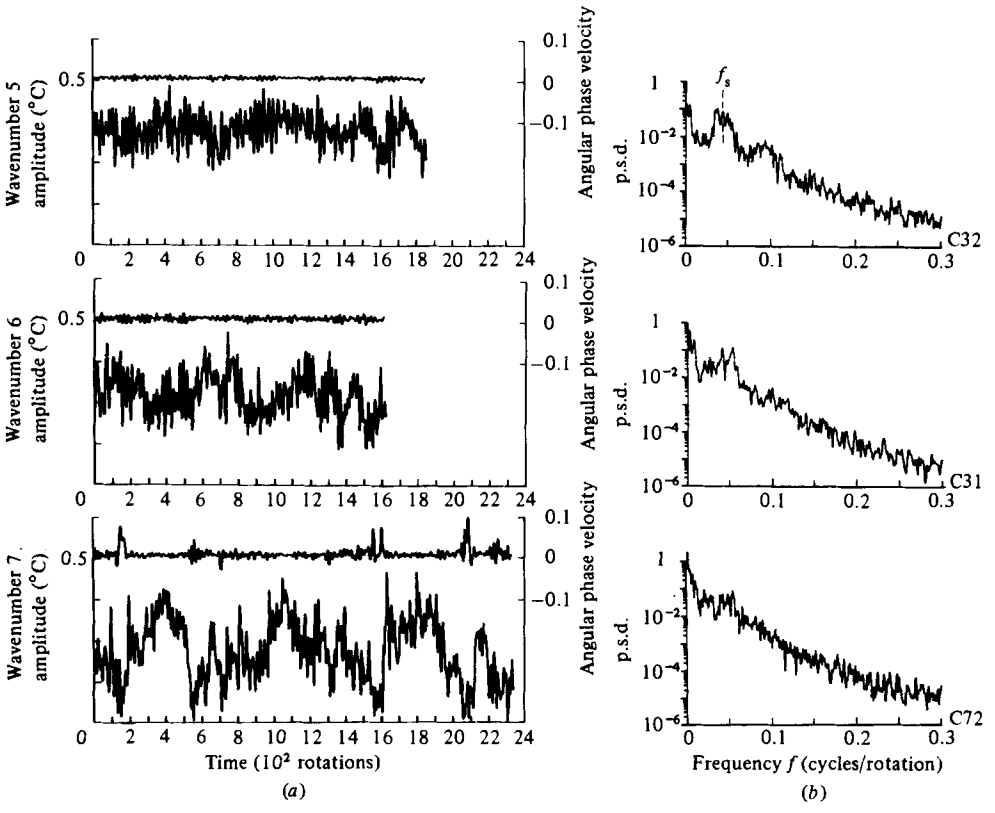

FIGURE 10. Temporal characteristics of dominant zonal wavenumbers in each experiment in the transition zone: (*a*) amplitudes and angular phase velocities as a function of time are shown in the lower and upper portions of each diagram respectively (angular phase velocity is in cycles per rotation, with positive values indicating counterclockwise motion relative to the annulus); (*b*) frequency spectra of wave amplitudes (p.s.d. is in °C² per unit frequency).

velocity characteristics are generally similar to those in the last experiment of the preceding region. The signal has a well-defined mean with intermittent oscillations; the mean value corresponds to the frequency f_1. The oscillation in the wave amplitude appears more aperiodic and less well-modulated. We also observe the emergence of weak low-frequency oscillations. The entire length of this and each of the other records is shown here to illustrate more clearly the presence of these low-frequency oscillations. The frequency spectrum appears like a somewhat-degenerate example of that characterizing structural vacillation. A broad peak is still evident and it is still possible to determine a mean frequency f_s. This broad band, however, exhibits substantial splitting. As in the frequency spectra at a single location, the background signal contains a larger percentage of the total power than in the preceding experiment. There is also considerable p.s.d. in the lower-frequency end of the spectrum.

In the next experiment, C31, the mean value of the angular phase velocity is again equivalent to the frequency f_1, and the oscillations around this mean appear more irregular. The fluctuation of the dominant wave amplitude is considerably more irregular, its mean value is lower and the variance about the mean is larger than in the preceding experiment. Note also the increased amplitude of the low-frequency

oscillations. The frequency spectrum of this record shows only a trace of the broad peak identified by f_s; the background signal and the broad peak have effectively merged.

In the last experiment in this sequence, C72, the angular phase velocity shows intermittent and large departures from a record which is otherwise similar to that in the preceding experiment. The fluctuations in the wave amplitude appear more irregular than in the previous experiment, and the low-frequency fluctuations have increased in magnitude to the point where the wave amplitude on occasions approaches zero. The large, intermittent fluctuations in the angular phase velocity correspond to the times when the wave amplitude is near zero and the error in the measurement of the phase velocity is large. The average angular phase velocity over the entire record no longer corresponds to the peak denoted by f_1 in figure 9(*b*), although an average calculated over portions of the record which exclude these large departures does correspond to this frequency. Hence we can still associate the peak f_1 with the drift of the dominant wave when its amplitude has moderate to large values. The frequency spectrum of the dominant wave shows practically no trace of the broad peaks observed in the preceding experiments. The spectrum appears broadband with a monotonic decrease of p.s.d. with increasing frequency.

When the amplitude of the dominant wavenumber, 7, is near zero, another wavenumber, 6, attains large amplitude. Note that the time-averaged amplitude of wavenumber 6 is comparable to, but less than, that of wavenumber 7 (figure 9*c*, experiment C72). When the amplitude of wavenumber 6 is moderate, its average angular phase velocity corresponds to the slightly weaker frequency peak to the left of f_1 in figure 9(*b*). Hence this second peak has the same meaning as the peak marked, f_1. Note, however, that these two waves of comparable magnitude, wavenumbers 7 and 6, do not coexist simultaneously with comparable magnitudes, but instead take their turn at being the dominant wave in the course of the experiment, 7 being dominant more often than 6. The amplitudes of the other wavenumbers in the vicinity of the major peak in the zonal-wavenumber spectrum are considerably lower. The angular phase velocities of these waves appear more irregular rather than intermittent, and their average values cannot be related to any other peaks in the frequency spectrum of the temperature record at a single location.

3.4. *Geostrophic-turbulence regime*

The sequence of temperature records, frequency and wavenumber spectra characterizing the geostrophic turbulence regime is shown in figure 11. Similar information for experiment C72, discussed in §3.3, is included for comparison. The data for this figure were derived from measurements at the same locations as used in the amplitude-vacillation experiments (viz near mid-depth and mid-gap of the annulus). There is no longer any particular advantage in examining the data near the one-quarter gap location as was done in the structural-vacillation and transition regions.

Qualitatively, the temperature–time records appear chaotic with a substantial low-frequency signal superimposed on the higher frequencies. The frequency spectra are all relatively featureless with a broad monotonic decrease of p.s.d. with frequency and no distinguishable peaks in the spectra which could be related to the phase drift of the dominant zonal wavenumbers. The zonal-wavenumber spectra display a broad distribution of energy with wavenumber, with relatively broad peaks and, at high wavenumbers, a nominal -4-power dependence of energy density on wavenumber. The power relationship is indicated by a straight line adjacent to the data in each of the experiments in the sequence, determined by a least-squares fit of the data. The

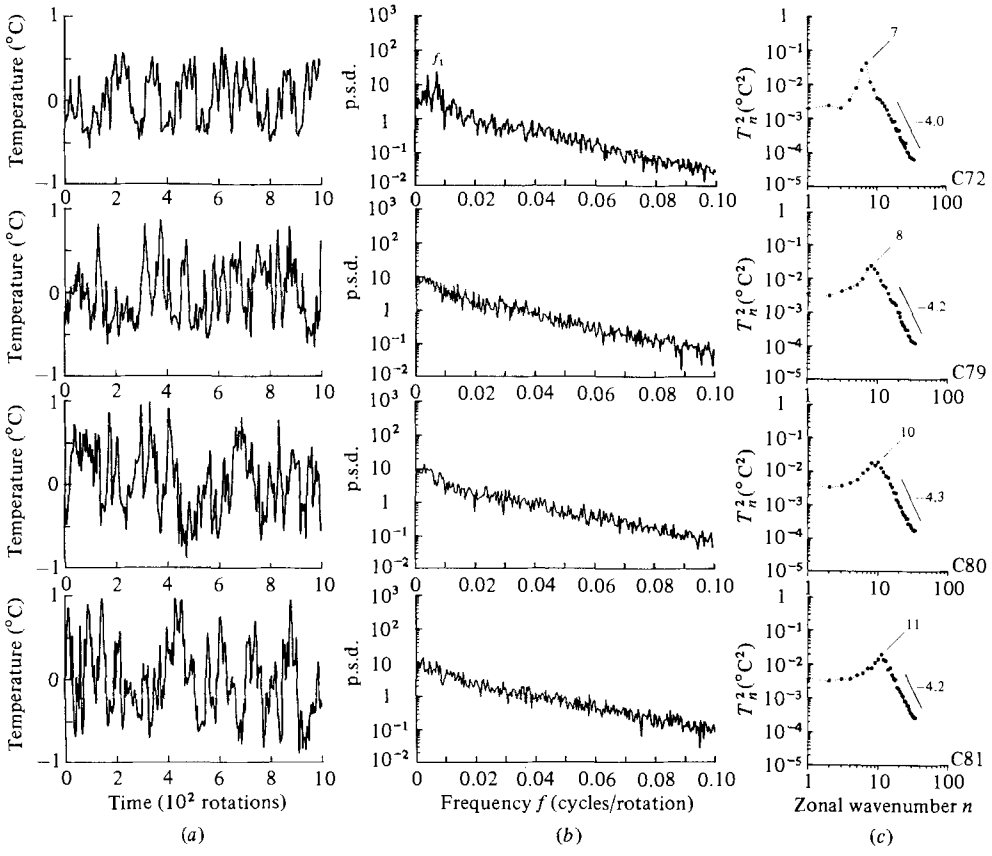

FIGURE 11. Characteristics of the geostrophic-turbulence regime: (*a*) time records of temperature departures from the mean at a single location near mid-depth and mid-gap (only the first 1000 rotations are shown here); (*b*) frequency spectra of the temperature records (p.s.d. is in °C² per unit frequency); (*c*) time-averaged zonal-wavenumber spectra obtained from interpolated temperature data at mid-depth and the same radius as the time records in (*a*).

numerical value of the slope of each such line is given in the figure, and the 95% confidence limits on the determination of these slopes are given in table 2. The wavenumber range for the determination of the slopes (also given in table 2) excludes the near vicinity of the broad peak, typically seven wavenumbers beyond the dominant wavenumber, as well as the last six wavenumbers, 31–36, where the spectra tend to be flattened owing to experimental noise, which is magnified at this limit of resolution. The information in figure 11 and table 2 suggests that there is no significant trend in the slopes of the wavenumber spectra as a function of rotation rate at constant imposed ΔT within the parameter range we have examined.

It is of interest to examine further the behaviour of the spectra in the geostrophic-turbulence regime over a broader range of parameters. Accordingly, we have analysed two additional experiments in the C-series, one at a larger and the other at a smaller imposed ΔT (20 and 5 °C, experiments C97 and C42 respectively). Both of these experiments were performed at the same rotation rate as that of C81, the highest rotation rate in the series. Their relative positions in dimensionless parameter space are shown in figure 1. The zonal-wavenumber spectra for C97, C81 and C42 are shown in figure 12, where we have normalized the abscissa by the wavenumber with the

Experiment	ΔT (°C)	Ω (s^{-1})	Ro_T	Ta (10^6)	Wavenumber range	Slope	95 % confidence limits on slope
97	20	1.57	0.172	21.6	14–30	−4.68	±0.19
72	10	1.05	0.193	9.61	14–30	−3.97	±0.34
79	10	1.26	0.134	13.8	15–30	−4.15	±0.26
80	10	1.40	0.109	17.0	17–30	−4.28	±0.26
81	10	1.57	0.086	21.6	17–30	−4.20	±0.23
42	5	1.57	0.040	16.5	21–30	−3.23	±0.60

TABLE 2. Values of the slopes and 95 % confidence limits; wavenumber spectra, C-series experiments, geostrophic-turbulence regime

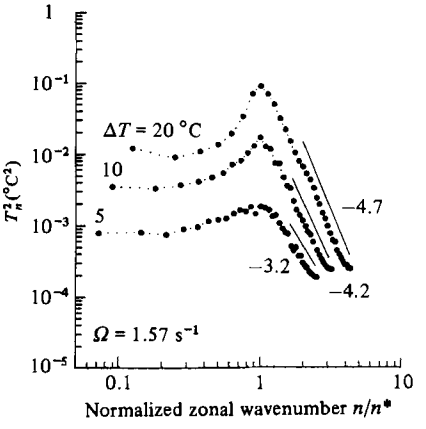

FIGURE 12. Zonal-wavenumber spectra for three different temperature contrasts, $\Delta T = 20$ °C (experiment C97), 10 °C (C81), and 5 °C (C42) at the same rotation rate $\Omega = 1.57\ s^{-1}$. The wavenumber axis is normalized by the wavenumber with the maximum energy, n^*, in order to display all three spectra on the same diagram. The wavenumber n^* is 8, 11 and 14 for experiments at $\Delta T = 20$, 10 and 5 °C respectively.

maximum energy in order to display all three spectra on the same diagram. The 95 % confidence limits on the slopes are given in table 2. Here we see convincing evidence of a systematic decrease in the spectral slope with decreasing imposed ΔT at constant rotation rate.

If geostrophic turbulence were 'frozen', the relationship between energy density and frequency should be the same as that between energy density and wavenumber. It is therefore of interest to plot the frequency spectra on a log–log scale over the entire range of frequencies defined by the data, and to examine the slopes at high frequency. Figure 13 shows such spectra, smoothed by two passes of hanning in order to reveal the slopes more clearly. The frequency spectra in figure 13(*a*) correspond to the sequence of experiments at successively higher rotation rates at constant imposed ΔT. The ones in figure 13(*b*) correspond to the experiments at different imposed temperature contrasts at the same rotation rate. All of these frequency spectra are averages of the spectra determined at the 9 individual thermistor locations, equally spaced in azimuth at the same radius and depth in the fluid. Since there is no known azimuthal bias in the annulus, as there is, for example, in the Earth's atmosphere due to topographic irregularities and land–sea differences, we should expect the spectra at different azimuths to be the same. In each experiment, however,

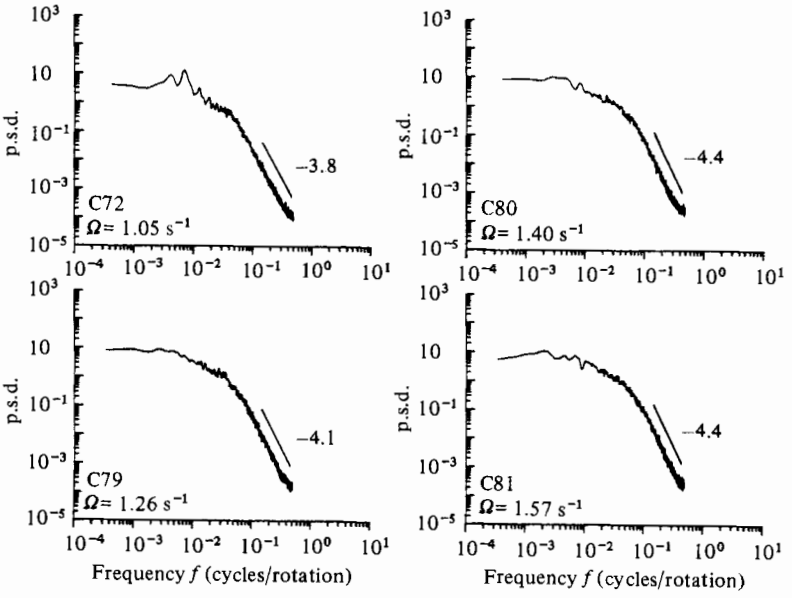

(*a*)

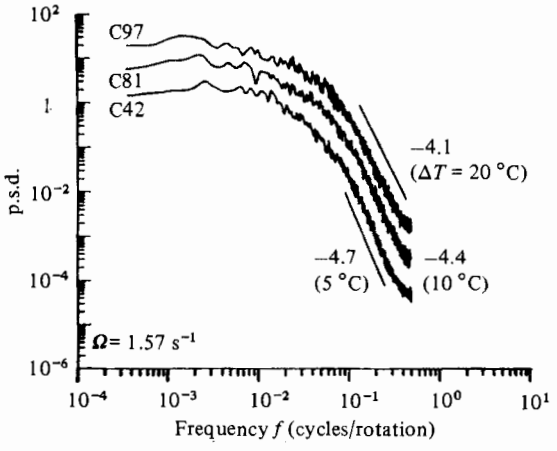

(*b*)

FIGURE 13. Frequency spectra over the entire observed frequency range in the geostrophic-turbulence regime: (*a*) spectra at different rotation rates, $\Omega = 1.05$ s^{-1} (experiment C72), 1.26 s^{-1} (C79), 1.40 s^{-1} (C80) and 1.57 s^{-1} (C81), and the same imposed temperature contrast $\Delta T = 10$ °C; (*b*) spectra at different imposed temperature contrasts, $\Delta T = 20$ °C (experiment C97), 10 °C (C81) and 5 °C (C42), and the same rotation rate $\Omega = 1.57$ s^{-1}.

the slopes at the 9 different azimuths departed significantly enough from their mean that the 95 % confidence intervals around the means for the different experiments, given in table 3, overlap one another. We must therefore conclude that our data do not establish the existence of a trend in the slopes of the frequency spectra with changes in the imposed ΔT at constant rotation rate, or with changes in the rotation rate at constant imposed ΔT. It would appear from comparison of figures 12 and 13 (*b*), taking into account the confidence limits reported in tables 2 and 3, that geostrophic turbulence is not 'frozen'.

Experiment	ΔT (°C)	Ω (s^{-1})	Ro_T	Ta (10^8)	Mean slope (average of 9 points)	95 % confidence limits on the mean
97	20	1.57	0.172	21.6	−4.14	±0.20
72	10	1.05	0.193	9.61	−3.82	±0.20
79	10	1.26	0.134	13.8	−4.15	±0.25
80	10	1.40	0.109	17.0	−4.40	±0.24
81	10	1.57	0.086	21.6	−4.38	±0.20
42	5	1.57	0.040	16.5	−4.68	±0.45

TABLE 3. Values of the mean slopes (average of 9 points) and 95 % confidence limits on the means; frequency spectra, C-series experiments, geostrophic-turbulence regime. The frequency range over which these slopes were determined is $0.1 < f < 0.3$ cycles per rotation.

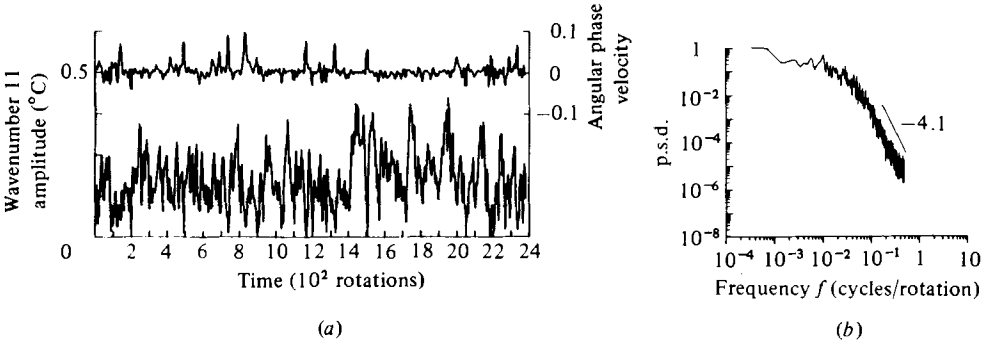

FIGURE 14. Temporal characteristics of the dominant zonal wavenumber 11 in geostrophic-turbulence experiment C81 : (*a*) amplitude and angular phase velocity as functions of time are shown in the lower and upper portions of the figure respectively (angular phase velocity is in cycles per rotation, with positive values indicating counterclockwise motion relative to the annulus); (*b*) frequency spectrum of the wave amplitude (p.s.d. is in °C² per unit frequency).

In the wave regime, and in most of the transition region, the wavenumber that was dominant in the time average remained dominant throughout the entire experiment. This is not the case in geostrophic turbulence, where other wavenumbers in the relatively broad spectral peak become dominant over short intervals of time (as shown, for example, in figure 9 (*d*) of Pfeffer *et al.* 1980*a*). We find, however, that the different wavenumbers in the broad spectral peak display similar behaviour. We will therefore examine the time variations of the phase velocity and amplitude of the dominant wavenumber, 11, in experiment C81 (upper and lower curves respectively in figure 14*a*) as representative of those in geostrophic turbulence.

In contrast with the periodic, semiperiodic and intermittent behaviour in the previous experiments, the phase velocity and amplitude of the dominant mode in geostrophic turbulence display irregular, aperiodic behaviour. Although the mean phase velocity is positive, indicating wave drift in the direction of rotation (counterclockwise), this mean no longer corresponds to any peak in the frequency spectrum of the temperature at a point in the fluid (figure 11*b*). Moreover, the fluctuations about the mean are considerable, including negative phase velocities for short intervals of time. The frequency spectrum of wavenumber 11, smoothed by two passes of hanning, is shown in figure 14 (*b*). It is remarkably similar to the frequency spectrum of the temperature at a point, displaying a nominal −4-power relationship between energy density and frequency in the high-frequency range.

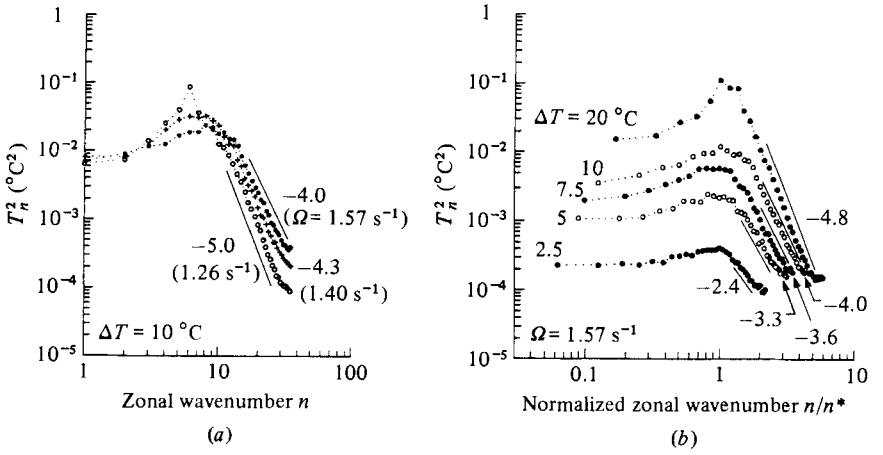

FIGURE 15. Zonal-wavenumber spectra in the D-series experiments: (*a*) spectra at different rotation rates, $\Omega = 1.26$ s^{-1} (experiment D41), 1.40 s^{-1} (D42) and 1.57 s^{-1} (D43), and the same imposed temperature contrast $\Delta T = 10$ °C; (*b*) spectra at different imposed temperature contrasts, $\Delta T = 20$ °C (experiment D69), 10 °C (D43), 8.5 °C (D50), 5 °C (D57) and 2.5 °C (D63), and the same rotation rate $\Omega = 1.57$ s^{-1}. The wavenumber axis is normalized by the wavenumber with the maximum energy, n^*, in order to display all three spectra on the same diagram. The wavenumber n^* is 6, 8, 10 and 16 for experiments at $\Delta T = 20$, 10, 7.5 and 2.5 respectively. In the experiment at $\Delta T = 5$ °C, n^* was taken as 11 instead of the wavenumber with the maximum energy to avoid crowding of the data at the high-wavenumber end of the spectrum.

In order to obtain more information about the structure of geostrophic turbulence, we estimated time-averaged wavenumber spectra in the D-series, where experiments were conducted over a broader range of parameters using a network that contained 72 equally spaced thermistors at mid-depth and at 0.44 gap width, measured from the inner cylinder. This network was designed to provide more accurate estimates of wavenumber spectra, since it provided 72 temperature readings around the circle, with no interpolated values. In this series, there were 11 experiments in the geostrophic-turbulence regime at various imposed temperature contrasts and rotation rates. Figure 15(*a*) shows the zonal wavenumber spectra at three points in dimensionless parameter space with the same imposed temperature contrast and rotation rates as experiments C79, C80 and C81 in the C-series. The 95 % confidence limits on these slopes are given in table 4. Unlike the results for the C-series, where the confidence limits (table 2) were larger (probably because the temperatures were interpolated rather than directly measured at all 72 points), these spectra display a weak, but definite, trend toward smaller slopes with increasing rotation rate which is significant at the 95 % level.

Figure 15(*b*) shows the zonal-wavenumber spectra at different imposed temperature contrasts in the D-series at the same rotation rate as the C-series experiments whose spectra are plotted in figure 12. The characteristics of the spectra are the same in both series. With decreasing imposed temperature contrast there is a trend toward broader peaks, flatter spectra at low wavenumbers and smaller slopes at high wavenumbers. This trend continues down to imposed $\Delta T = 2.5$ °C. The 95 % confidence limits on the slopes (table 4) reveal some overlap (i.e. the interval for $\Delta T = 7.5$ °C overlaps the intervals for $\Delta T = 10$ °C and $\Delta T = 5$ °C), but the overall trend seems well established by the data.

In figure 16 we show the location of each of the D-series experiments in the geostrophic-turbulence regime as a function of imposed thermal Rossby and Taylor

Experiment	ΔT (°C)	Ω (s^{-1})	Ro_T	Ta (10^8)	Wave number range	Slope	95% confidence limits on slope
69	20	1.57	0.172	21.6	12–30	−4.82	±0.15
41	10	1.26	0.134	13.8	14–30	−4.95	±0.13
42	10	1.40	0.109	17.0	14–30	−4.31	±0.15
43	10	1.57	0.086	21.6	16–30	−3.98	±0.14
49	7.5	1.26	0.101	13.8	15–30	−4.15	±0.09
50	7.5	1.57	0.064	21.6	18–30	−3.61	±0.26
56	5.0	1.26	0.067	13.8	16–30	−3.44	±0.17
57	5.0	1.57	0.043	21.6	18–30	−3.28	±0.26
61	2.5	0.96	0.058	8.1	14–30	−2.72	±0.17
62	2.5	1.26	0.034	13.8	18–30	−2.82	±0.29
63	2.5	1.57	0.022	21.6	23–30	−2.35	±0.29

TABLE 4. Values of the slopes and 95% confidence limits; wavenumber spectra, D-series experiments, geostrophic-turbulence regime

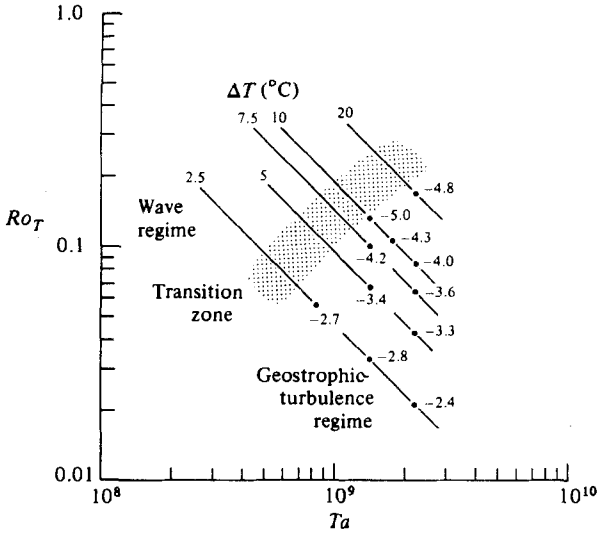

FIGURE 16. Slope of the wavenumber spectrum at high zonal wavenumbers as a function of imposed thermal Rossby and Taylor numbers in the geostrophic-turbulence regime of the D-series experiments. The location of each experiment is designated by a dot, and its slope is indicated adjacent to it.

numbers. At each location we show the slope of the spectrum at high wavenumbers. There appears to be a definite trend toward smaller slopes with lower thermal Rossby number which is most pronounced at high Taylor numbers. This trend is displayed more clearly in figure 17. This result seems to differ from that predicted by the much-referenced geostrophic-turbulence theory of Charney (1971). This theory postulates an inertial subrange characterized by an enstrophy† cascade toward higher wavenumbers at scales which are much smaller than those excited by baroclinic instability. In the inertial subrange the Reynolds numbers are considered to be

† Enstrophy is defined as one-half the mean-squared vorticity.

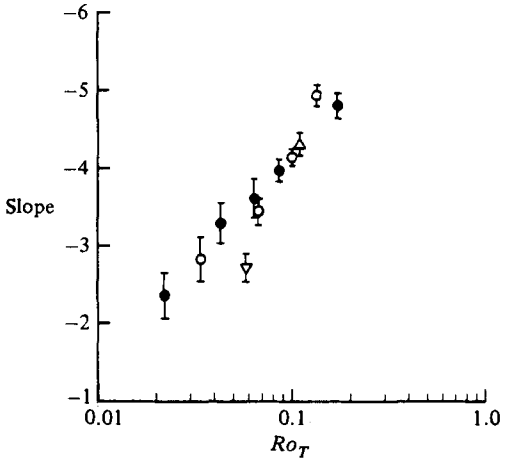

FIGURE 17. Slope as a function of thermal Rossby number in the D-series experiments. Like symbols correspond to the same rotation rate: ●, $\Omega = 1.57$ s^{-1}; △, 1.40 s^{-1}; ○, 1.26 s^{-1}; ▽, 0.96 s^{-1}.

sufficiently large such that internal viscous dissipation is negligible. It is further assumed that, away from the boundary layer, the turbulence is locally homogeneous and isotropic in horizontal planes and that boundary friction does not affect the turbulent motion at sufficiently high wavenumbers. Moreover wave components are considered to interact only with components of comparable wavenumber. It follows that the energy spectrum in such a range is proportional to n^{-3}. Other theories which take into account the effects of distortion and strain (e.g. Shabbar 1974), or the presence of fronts (e.g. Andrews & Hoskins 1978), lead to different power laws, but none contains a dependence on thermal Rossby number or Rossby radius of deformation. Further experiments are required, however, to confirm this dependence. In particular, we must be able to measure the spectrum at higher wavenumbers in the experiments at small thermal Rossby number in which the energy peak associated with the baroclinic excitation scale is broad and is centered at relatively high wavenumbers not too far from the cut-off scale of the current measurements. This can best be done by using streak photography in place of thermistors for velocity measurements down to scales smaller than the resolution of our thermistor network.

4. Summary

As we have seen, the route to geostrophic turbulence in our experiments proceeds in a series of steps as the rotation rate of the container (the externally imposed parameter) is increased from low to high values. The first departure from axisymmetric zonal flow occurs in the form of wave-amplitude vacillation, a doubly periodic phenomenon whose spatial structure is described essentially by a single zonal wavenumber and its lower-amplitude sidebands and higher harmonics.

As the rotation rate of the container is further increased, amplitude vacillation gives way abruptly to structural vacillation, a phenomenon with a fundamentally different kind of temporal behaviour, but with spatial characteristics that continue to be described by a single zonal wavenumber and its higher harmonics. The sidebands play a lesser role here with respect to the higher harmonics, which become more pronounced with increased rotation rate. The frequency spectrum of the temperature record at a single location resembles that for a singly periodic phenomenon, with superimposed background noise which increases with increasing rotation

rate. In certain respects this spectrum appears simpler than that for amplitude vacillation. This is because the counterclockwise drift of the wave pattern masks the relatively lower-amplitude, semiperiodic fluctuations associated with the radial oscillation of the wave-energy centres. These fluctuations reveal themselves, however, in the time record and frequency spectrum of the dominant wave amplitude near one-quarter gap width in the annulus. The latter spectrum is characterized by broad peaks centred on frequency f_s and its higher harmonics, where f_s is the mean frequency of the radial oscillation of the wave-energy centres. This frequency is incommensurate with the wave-drift frequency. It is therefore tempting to describe structural vacillation as a doubly periodic phenomenon. Since the peaks around f_s are broad, however, this form of vacillation cannot be considered doubly periodic, and is, in fact, a more complex phenomenon than amplitude vacillation.

At higher rotation rates, before we reach fully developed geostrophic turbulence, there is a region in dimensionless-parameter space which we have designated as a transition zone. In this zone the background signal, which first emerged in structural vacillation and increased slightly with rotation rate, becomes increasingly prominent in the time records and in the frequency and wavenumber spectra of both the temperature record at a single location and of the wave amplitude. In the frequency spectra it gradually merges with the dominant peaks to give a final broadband shape of the spectra as we progress into geostrophic turbulence. In the wavenumber spectra the background signal merges with the higher harmonics, the dominant peak broadens, but does not disappear, and the energy in the low-wavenumber end of the spectra begins to increase. This progressive peak-broadening and increase in the energy at low wavenumbers continues into geostrophic turbulence. The energy level in the lowest wavenumbers, which was two orders of magnitude smaller than that in the dominant wave in the wave regime, becomes lower by only a factor of two in the experiment that is deepest in the geostrophic-turbulence regime (experiment D63, $\Delta T = 2.5$ °C, $\Omega = 1.575$ s^{-1}, figure 15*b*).

The dominant peak in the zonal-wavenumber spectrum is a consequence of the baroclinic-instability mechanism which is central to these experiments. The baroclinic scale is the one at which basic-state available potential energy is fed into the wave motion and converted into wave kinetic energy. The change of this wave scale with thermal Rossby and Taylor numbers and the broadening of the peak in the wavenumber spectrum are consistent with linear baroclinic-instability theory, which also predicts more complicated radial structure with decreasing thermal Rossby number and increasing Taylor number (see Pfeffer *et al.* 1980*b*).

In the geostrophic-turbulence regime we find a nominal -4-power dependence of energy density on *frequency* which does not appear to be sensitive to changes in Rossby and Taylor number. Our data, however, reveal an n-power dependence of energy density on *wavenumber* which shows a significant dependence on thermal Rossby number, ranging from $n = -4.82 \pm 0.15$ at $Ro_T = 0.172$ to $n = -2.35 \pm 0.29$ at $Ro_T = 0.022$. If these results are confirmed in other experimental studies, they would point to the need for a new theory of geostrophic turbulence.

This research was supported by the Office of Naval Research (N00014-77-C-0265). We are also grateful to the Computing Centers at Florida State University and at the National Center for Atmospheric Research for providing computer time for the computations presented in this paper. The National Center for Atmospheric Research is supported by the National Science Foundation. This paper is contribution no. 201 of the Geophysical Fluid Dynamics Institute.

REFERENCES

ANDREWS, D. G. & HOSKINS, B. J. 1978 Energy spectra predicted by semi-geostrophic theories of frontogenesis. *J. Atmos. Sci.* **35**, 509–512.

CHARNEY, J. G. 1971 Geostrophic turbulence. *J. Atmos. Sci.* **28**, 1087–1095.

FENSTERMACHER, P. R., SWINNEY, H. L. & GOLLUB, J. P. 1979 Dynamical instabilities and the transition to chaotic Taylor vortex flow. *J. Fluid Mech.* **94**, 103–128.

FOWLIS, W. W. & PFEFFER, R. L. 1969 Characteristics of amplitude vacillation in a rotating, differentially heated fluid determined by multi-probe technique. *J. Atmos. Sci.* **26**, 100–108.

GOLLUB, J. P. & BENSON, S. V. 1980 Many routes to turbulent convection. *J. Fluid Mech.* **100**, 449–470.

HIDE, R. & MASON, P. J. 1975 Sloping convection in a rotating fluid. *Adv. Phys.* **24**, 47–100.

HIDE, R., MASON, P. J. & PLUMB, R. A. 1977 Thermal convection in a rotating fluid subject to a horizontal temperature gradient: spatial and temporal characteristics of fully developed baroclinic waves. *J. Atmos. Sci.* **34**, 930–950.

LINDZEN, R. S., FARRELL, B. & JACQMIN, D. 1982 Vacillation due to wave interference: applications to the atmosphere and to annulus experiments. *J. Atmos. Sci.* **39**, 14–23.

MOROZ, I. M. & BRINDLEY, J. 1982 An example of two-mode interaction in a three-layer model of baroclinic instability. *Phys. Lett.* **91A**, 226–230.

PFEFFER, R., BUZYNA, G. & FOWLIS, W. W. 1974 Synoptic features and energetics of wave-amplitude vacillation in a rotating, differentially-heated fluid. *J. Atmos. Sci.* **31**, 622–645.

PFEFFER, R. L., BUZYNA, G. & KUNG, R. 1980*a* Time-dependent modes of behavior of thermally driven rotating fluids. *J. Atmos. Sci.* **37**, 2129–2149.

PFEFFER, R. L., BUZYNA, G. & KUNG, R. 1980*b* Relationships among eddy fluxes of heat, eddy temperature variances and basic-state temperature parameters in thermally driven rotating fluids. *J. Atmos. Sci.* **37**, 2577–2599.

RAO, S. T. & KETCHUM, C. B. 1975 Spectral characteristics of the baroclinic annulus waves. *J. Atmos. Sci.* **32**, 698–711.

RAO, S. T. & KETCHUM, C. B. 1976 Spectral properties of the baroclinic waves in an annulus with a rigid upper surface. *J. Atmos. Sci.* **33**, 1067–1072.

RHINES, P. G. 1979 Geostrophic turbulence. *Ann. Rev. Fluid Mech.* **11**, 401–410.

SHABBAR, M. 1974 Inertial ranges in three-dimensional quasi-geostrophic turbulence. *Boundary-Layer Met.* **6**, 413–421.

WHITE, H. D. & KOSCHMIEDER, E. L. 1981 Convection in a rotating, laterally heated annulus. Pattern velocities and amplitude oscillations. *Geophys. Astrophys. Fluid Dyn.* **18**, 301–320.